Conference Paper, Published Version

Kimura, Ichiro; Ishigaki, Taisuke; Hiroe, Masanori

Numerical Simulation of 3D Turbulent Flow structures around an Attracting Groin with Local Scour

NUMERICAL SIMULATION OF 3D TURBULENT FLOW STRUCTURES AROUND AN ATTRACTING GROIN WITH LOCAL SCOUR

ICHIRO KIMURA[†]

Department of Civil and Environmental Engineering, Matsue National College of Technology
14-4 Nishi-ikuma, Matsue 690-8518, Japan

TAISUKE ISHIGAKI

Disaster Prevention Research Institute, Kyoto University
Fushimi, Kyoto 612-8235, Japan

MASANORI HIROE

West Japan Railway Company
4-24, Shibata 2-chome Kita-ku, Osaka 530-8341, Japan

Prediction of flow structures around an attracting groin, of which head is shifted toward downstream, is important because such groin has a disadvantage in a submerged situation, namely, the flow over the groin attacks a bank and erodes it. In this paper, 3D turbulent flow structures around an attracting groin with scour hole are studied numerically. The basic equations on generalized curvilinear movable coordinate are used to consider the complex topography and free surface elevation. A refined non-linear k-ε model is adopted as a turbulence model in order to reproduce secondary currents of second kind and a vortex formations. The computational conditions are same as those of the laboratory tests by Ishigaki et al (2003). The numerical results show that the fundamental turbulence structres with a circular flow, which may be a main trigger of the local scour, can be reasonably predicted by the present model.

1 Introduction

In recent years, groins are set not only for the protection of riverbank erosion but also for the environmental preservation in Japan. Groins have a function to form a varied bed configuration as well as a function to deflect a flow and reduce velocity near the riverbank. The recent groins are usually set perpendicular to a riverbank, which is called a deflecting groin. On the other hand, many old groins in Japan were set at angles to a riverbank. The groin which head is shifted toward downstream is called attracting groin and is not commonly used in a submerged situation because a flow over the groin attacks a bank and erodes it. Ishigaki et al (2003) studied the flow structures around a old attracting groin built about 400 years ago in Kyoto Prefecture and pointed out that the scour hole depends on the hydraulic condition and that there is a hydraulic condition for preventing severe bank erosion. They also referred to the possibility that the scour hole caused by the flow around an attracting groin functions as a biotope. Those results

[†] Work partially supported by Grant in Aid for Scientific Research, JSPS, No.14750433..

indicate that the attracting groin can be useful both for flood control and environment under certain hydraulic conditions. Therefore, it is very important to predict the flow structures and bed configuration around an attracting groin. A numerical simulation with RANS type modeling for turbulence has been recognized as a powerful tool to predict detailed 3D flow structures around bluff bodies. Kimura and Hosoda (2003) proposed a modified non-linear k-ε model through the consideration of realizability and applied it to the flows around a rectangular cylinder. Kimura et al (2002, 2003) modified the same turbulence model to a generalized curvilinear form and applied it to the flow around upstream / downstream inclined sub-merged groins. Those studies showed that the non-linear k-ε model could predict not only time-mean flow structures but also unsteady flow structures such as vortex shedding from the tip of groins with practical accuracy. In this study, characteristics of 3D turbulent flow structures around an attracting submerged groin with a scour hole are numerically investigated. A generalized curvilinear movable coordinate is employed to simulate the free surface oscillation and take into account the complex topography. The computations were performed under the conditions of the laboratory tests performed by Ishigaki et al (2003). The flow features around an attracting groin are discussed through the comparison of computational and experimental results.

2 Computational Model

2.1. *Governing Equations*

The Reynolds averaged 3D flow equations with contravariant components of velocity vectors on a generalized curvilinear movable coordinate system are used as governing equations in this study. The governing equations are described as

$$\frac{1}{\sqrt{g}}\frac{\partial V^{\alpha}\sqrt{g}}{\partial \xi^{\alpha}} = 0 \tag{1}$$

$$\frac{\partial V^i}{\partial t} + \nabla_j\left[V^i(V^j - W^j)\right] + V^i\nabla_j W^j + V^j\nabla_j W^i = F^i - \frac{1}{\rho}g^{ij}\nabla_j p + \nabla_j\left[-\overline{v^i v^j}\right] + 2\nu\nabla_j e^{ij} \tag{2}$$

$$\frac{\partial k}{\partial t} + \nabla_j\left[k(V^j - W^j)\right] + k\nabla_j W^j = -g_{il}\overline{v^l v^j}\nabla_j V^i - \varepsilon + \nabla_j\left\{\left(\frac{D_t}{\sigma_k} + \nu\right)g^{ij}\nabla_i k\right\} \tag{3}$$

$$\frac{\partial \varepsilon}{\partial t} + \nabla_j\left[\varepsilon(V^j - W^j)\right] + \varepsilon\nabla_j W^j = -C_{\varepsilon 1}\frac{\varepsilon}{k}g_{il}\overline{v^l v^j}\nabla_j V^i - C_{\varepsilon 2}\frac{\varepsilon^2}{k} + \nabla_j\left\{\left(\frac{D_t}{\sigma_k} + \nu\right)g^{ij}\nabla_i \varepsilon\right\} \tag{4}$$

where ξ^j = generalized curvilinear coordinate, t = time, V^i = contravariant component of the velocity vector of flows, W^i = contravariant component of the velocity vector of grid motion, p = pressure, ν = molecular dynamic viscosity, ρ = density of water, k = turbulent energy, ε = turbulent energy dissipation rate, g_{ij} and g^{ij} = covariant and

contravatiant component of metric tensor, $g = \det(g_{ij})$ and F^i = contravariant component of gravity acceleration. ∇^i indicates a covariant differential, for instance,

$$\nabla_i A^k = \frac{\partial A^k}{\partial \xi^i} + A^j \Gamma_{ij}^{\ k},\ \Gamma_{ij}^{\ k} = \left\{ \begin{matrix} k \\ i\ j \end{matrix} \right\} = \frac{1}{2} g^{km} \left(\frac{\partial g_{jm}}{\partial \xi^i} + \frac{\partial g_{im}}{\partial \xi^j} - \frac{\partial g_{ij}}{\partial \xi^m} \right) = \frac{\partial \xi^k}{\partial x^p} \frac{\partial^2 x^p}{\partial \xi^i \partial \xi^j} \quad (5)$$

where Γ_{ij}^{k} is a Christoffel symbol.

2.2. *Turbulence Model*

To calculate a complex turbulent flow with separation and vortex shedding, a 2nd-order non-linear k-ε model by Kimura and Hosoda (2003) is adopted as a turbulence model. The constitutive equations of the model are described as follows.

$$-\overline{v'^i v'^j} = D_t S^{ij} - \frac{2}{3} k \delta_s^i g^{sj} - \frac{k}{\varepsilon} D_t \left[\alpha_1 Q_1 + \alpha_2 Q_2 + \alpha_3 Q_3 \right],\ D_t = C_\mu \frac{k^2}{\varepsilon} \quad (6)$$

$$Q_1 = S^{i\alpha} g_{\alpha l} \Omega^{lj} + S^{j\beta} g_{\beta l} \Omega^{li} \quad (7)$$

$$Q_2 = S^{i\alpha} g_{\alpha l} S^{lj} - \frac{1}{3} S^{k\alpha} g_{\alpha m} S^{m\beta} g_{\beta k} \delta_l^i g^{lj},\ Q_3 = \Omega^{i\alpha} g_{\alpha l} \Omega^{lj} - \frac{1}{3} \Omega^{k\alpha} g_{\alpha m} \Omega^{m\beta} g_{\beta k} \delta_l^i g^{lj} \quad (8)$$

$$S^{ij} = g^{j\alpha} \nabla_\alpha V^i + g^{i\alpha} \nabla_\alpha V^j,\ \Omega^{ij} = g^{j\alpha} \nabla_\alpha V^i - g^{i\alpha} \nabla_\alpha V^j \quad (9)$$

The model coefficients are not constants but functions of the strain parameter S and the rotation parameter Ω. In this study, all the coefficients are given as functions with one variable M for simplicity as follows (Kimura and Hosoda, 2003).

$$C_\mu = \min\left[0.09,\ \frac{0.3}{1 + 0.09 M^2} \right],\ \alpha_1 = -0.1325 f_M,\ \alpha_2 = 0.0675 f_M,\ \alpha_3 = -0.0675 f_M \quad (10)$$

$$f_M = \frac{1}{1 + 0.02 M^2},\ M = \max[S, \Omega],\ S = \frac{k}{\varepsilon} \sqrt{\frac{1}{2} S^{i\alpha} g_{\alpha j} S^{j\beta} g_{\beta i}},\ \Omega = \frac{k}{\varepsilon} \sqrt{\frac{1}{2} \Omega^{i\alpha} g_{\alpha j} \Omega^{j\beta} g_{\beta i}} \quad (11)$$

In above equations, α_1-α_3 were adjusted through the consideration of the distribution of turbulent intensities in a simple shear flow compared with the previous experimental results. C_μ[M] was tuned to satisfy the realizability in a simple shear flow and singular points in both 2D and 3D flow fields.

2.3. *Outline of Numerical Method*

The differential equations governing the mean-velocities and the turbulence field are solved with the finite volume method on full-staggered grid system. The metric tensors and the Cristoffel symbols are defined only at grid points to save computer memory and the values at other positions are interpolated at each computational step.

QUICK scheme is applied to the convection terms and the central differencing is used for the diffusion terms in the momentum equations. The hybrid central upwind scheme is applied to the k and ε equations for the computational stability. Adams-

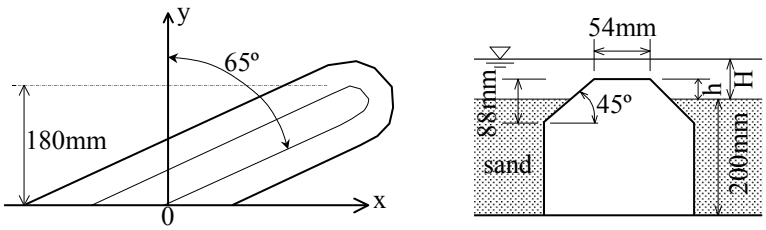

Figure 1. Attracting groin used in the laboratory test by Ishigaki et al (2003) (left:plan view, right:vertical view)

.

Table 1 Hydraulic parameters in the laboratlry test (Case A5) by Ishigaki et al (2003).

H/h	H (cm)	Q (l/s)	u_*/u_{*c}
1.92	9.48	17.38	0.83

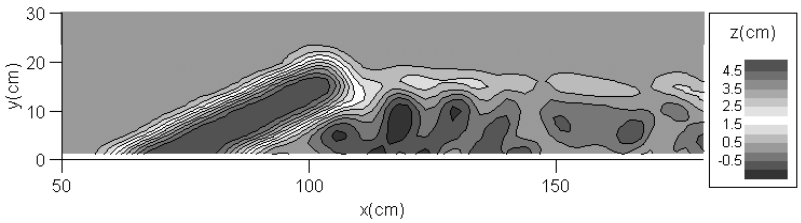

Figure 2. Bed configuration in Case-A5 in the laboratory test by Ishigaki et al (2003).

Bashforth scheme with second-order accuracy in time is used for time integration in each equation. The basic equations are discretized as fully explicit forms and are solved successively along the time axis step by step. The pressure field is solved using iterative procedure at each time step using SOLA algorithm.

2.4. *Boundary and Initial Conditions*

Since the present turbulence model is a high Reynolds number type, the wall function approach is applied as the wall boundary conditions for k and ε. The wall friction is evaluated by the log-law. At the downstream end of the computational domain, the longitudinal gradients of all variables are assumed to be zero. At the boundary inlet, the level of k is chosen to be $(0.02U_0)^2$ (U_0 = averaged velocity). The value of ε at the inlet is determined from the value of k at the inlet by specifying the ratio $D_t/\nu = 10$.

The free surface motion is solved by a simple relation in equation (12) since the contravariant components of the velocity vector are used in the basic equations.

$$\Delta h = \sqrt{g_{33}} V^3 \Delta t \tag{12}$$

where Δt = time increment and Δh = surface elevation during Δt. To consider the rapid attenuation of turbulent intensities in the depth-wise direction near the free surface, the eddy viscosity is multiplied by the following dumping function (Hosoda, 1990).

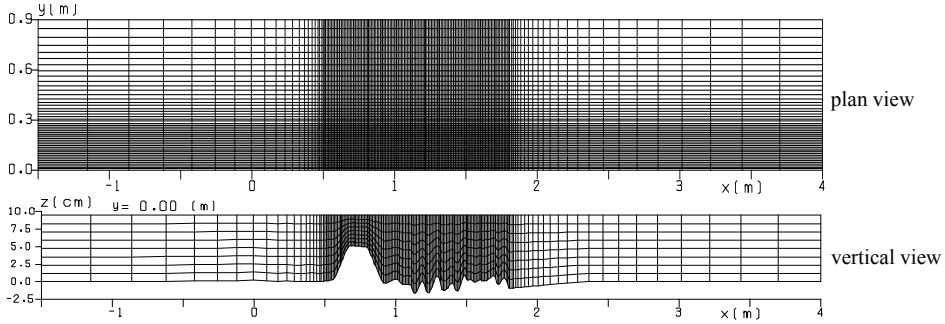

Figure 3. Plan and vertical views of numerical grid at y = 0cm (8-layers model).

$$f_s = 1 - \exp\left(- B \frac{(h-y)\varepsilon_s}{k_s^{3/2}} \right) \quad , \quad (B = 10) \tag{13}$$

where sub-*s* indicates the value at the surface. ε at the surface is evaluated by the following formula to calculate the secondary currents of 2nd kind (Sugiyama, 1995).

$$\varepsilon_s = \frac{C_{\mu 0}{}^{3/4} k_s^{3/2}}{0.4 \Delta y_s} , \ (C_{\mu 0} = 0.09) \tag{14}$$

At the beginning of the calculation, U (= velocity in the longitudinal direction (x-direction)) = U_0 (=averaged bulk velocity), V (= velocity in the transverse direction (y-direction) = 0, $k = k_{in}$ and $\varepsilon = \varepsilon_{in}$ (k_{in} and ε_{in} are the values of k and ε at the inlet boundary) are specified over the whole computational domain.

3 3D Computation of Flows around an Attracting Groin

3.1. *Computational Conditions*

Computations are performed under the conditions of the laboratory tests by Ishigaki et al (2003). The experiment was performed in a 10 m long, 0.9 m wide and 0.3 m deep straight flume. The middle part of the flume was made of movable bed filled with fine sand of which the mean diameter was 0.26mm. Fig. 1 shows the plan and cross-sectional view of the attracting groin model. The groin model was set on the right hand side bank of the experimental flume. The experiment was performed under 5 different submerged and non-submerged hydraulic conditions. The computation was performed under the conditions of Case A5 (submerged case). The hydraulic parameters in Case A5 were listed in Table 1. Fig.2 shows the bed topography in Case A5 at 1 hour after the beginning of the experiment. A scour hole is formed at the downstream area of the groin. The computation was performed under the fixed bed condition with the scour hole.

Fig. 3 shows plan and vertical views of the computational grid. The grid in the x-y plane was made using geometric series. The number of the grid in a horizontal plane is

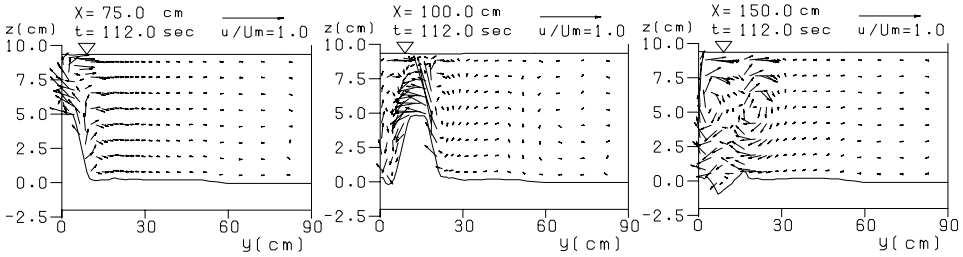

Figure 4. Cross-sectional flow patterns at x = 75, 100, 150 cm (8-layers model).

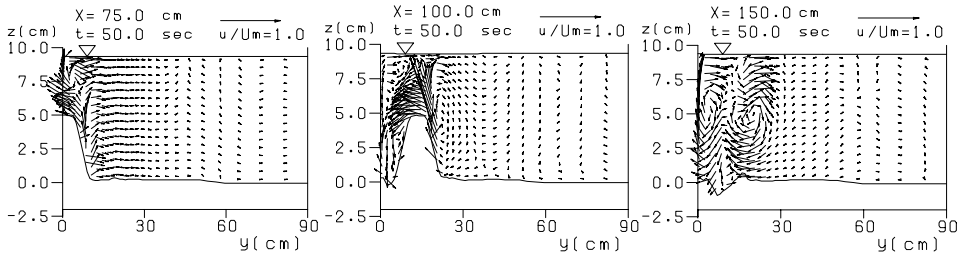

Figure 5. Cross-sectional flow patterns at x = 75, 100, 150 cm (16-layers model).

180 (x-direction) × 50 (y-direction). The grid in the z-direction was made by dividing the local depth into layers with equal thickness. To consider effects of a grid size, two grids with different layer number (8-layers and 16-layers) were tested. The vertical view of the grid (8-layers model) in the x-z plane at y = 0 cm is shown in Fig.3.

3.2. *Flow Patterns in Cross Sections*

Fig. 4 shows the cross-sectional flow patterns at x = 75, 100 and 150cm in the computational result (8-layers grid). The time of the result is at 112 seconds after the initial conditions. Note that the scale of the vertical direction is enlarged in these figures. The characteristic flow of attracting groin, namely, a strong flow toward the riverbank can be seen at x = 75 and 100cm. The flow tends toward the downward direction behind the groin and goes into the sour hole. The marked flows are likely to be a main cause of formations of the deep scour hole. The flow at x = 150cm forms two vortices in the clockwise direction. Fig.5 are the computational results in cross-sections at x = 75, 100 and 150cm with 16-layers grid. The flow patterns are similar to those in Fig.4. Therefore, the grid with 8-layers in a vertical direction is likely to be enough to reproduce fundamental flow structures. However, slight difference can be seen between two results, i.e., the flow separation behind the groin is only captured by the 16-layers grid.

3.3. *Flow Patterns in Vertical and Horizontal Sections*

Fig.6 (a) and (b) are computational velocity vectors with the 16-layers grid in vertical longitudinal sections at y = 1 and y = 10cm, respectively. These figures indicate that an upward flow is dominant near the side wall (y=1cm) at the downstream region of the

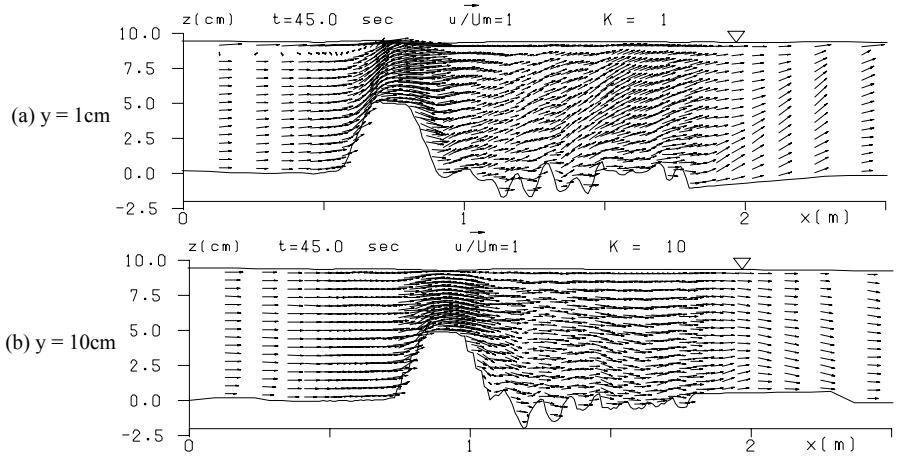

Figure 6. Flow patterns in vertical sections at y = 1, 10 cm (16-layers model).

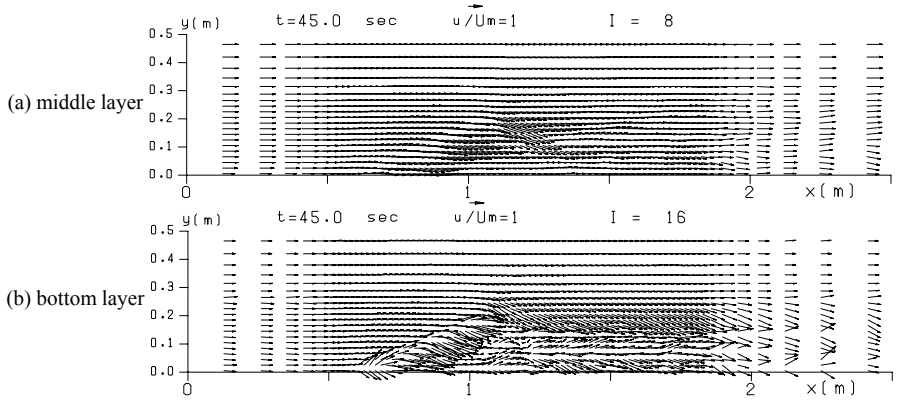

Figure 7. Plan views of flow patterns at middle and bottom layers (16-layers model).

groin, while a downward flow is dominant at the section of y = 10cm. The flow separation is not generated behind the groin in both sections.

Fig.7 (a) and (b) show the plan view of computational flow patterns with the 16-layer grid at the middle layer and at the bottom layer, respectively. The flow from the main channel toward the riverbank can be seen just downstream the groin at the middle layer. The flow toward the riverbank also can be seen over the groin at the bottom layer. The computational results demonstrate again the risk of attracting groins to erode the riverbank. The flow pattern near the bed at the downstream region of the groin is much disturbed because of the complex topography of the scour hole. Fig.8 shows the comparison of surface-velocity distributions in the longitudinal direction in the experimental and numerical results. In the experimental result, the velocity profile has an inflection point at the downstream area of the groin because the flow over the groin is decelerated near the head of the groin. The computation could capture the profile with an inflection point though the profile is damped more rapidly than the experimental result.

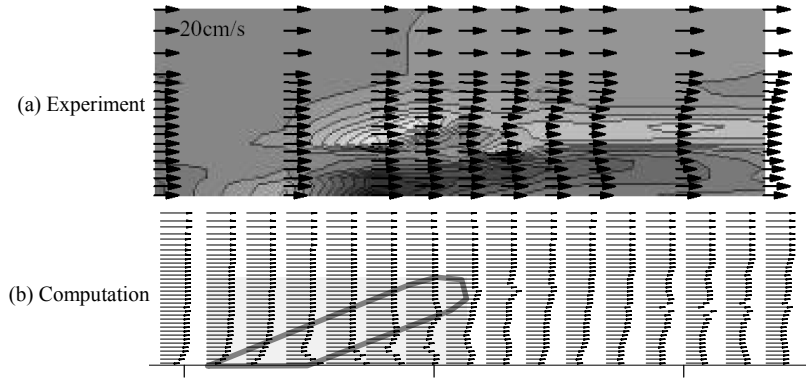

Figure 8. Comparison of stream-wise velocity distributions at a surface.

4 Conclusions

It is important that hydraulic engineers have to recognize the risk of attracting groin under a submerged condition and predict flow structures in detail in planning such groin. In this paper, 3D turbulent flow structures around an attracting groin with a scour hole were studied numerically. A modified non-linear k-ε model, which was tuned considering the realizability, was adopted as a turbulence model. A generalized curvilinear movable coordinate was used to consider the complicated bed topography and water surface elevation. Computations were performed under the conditions of the laboratory test by Ishigaki et al (2003). The computational results indicated that the present model could capture the fundamental aspects of 3D flow features, such as a flow which attacks a riverbank at the downstream region of an attracting groin.

References

Gatski, T.B. and Speziale, C.G.(1993). "On Explicit Algebraic Stress Models for Complex Turbulent Flows." *J. Fluid Mech*.,254, 59-78.

Hosoda, T., (1990). Ph.D. Thesis, Kyoto University (in Japanese).

Ishigaki, T., Ueno, T. and Tanaka, N. (2003). "Traditional Counter Measures for Flood in Kyoto District (2) – Experimental Study on Old Attracting Groin in Kameoka –." *Annuals of Disas. Prev. Res. Inst., Kyoto Univ*., 46(B) (in Japanese).

Kimura, I. and Hosoda, T.(2003). "A Non-linear k-ε Model with Realizability for Prediction of Flows around Bluff Bodies." *Int. J. Numer. Meth. Fluids*, 42, 813-837.

Kimura, I., Hosoda, T. and Onda, S. (2002). "Prediction of 3D Flow Structures Around Skewed Spur Dikes by Means of a Non-linear k-ε Model." *River Flow 2002* (eds. D.Bousmar and Y. Zech), Balkema, 1, 65-73.

Kimura, I., Hosoda, T., Onda, S. and Tominaga, A. (2003). "3D Numerical Analysis of Unsteady Flow Structures around Inclined Spur Dikes by Means of a Non-Linear k-ε Model." *Proc. of the Int. Symp. on Shallow Flows*, Delft, The Netherlands, Part III, 205-212.

Sugiyama, H., Akiyama, M. and Matsubara, T. (1995). "Numerical simulation of compound open channel flow on turbulence with a Reynolds stress model." *Journal of Hydraulic, Coastal and Environmental Engineering*, 515 / II-31: 55-65 (in Japanese).